Insight Gained from Using Machine Learning Techniques to Predict the Discharge Capacities of Doped Spinel Cathode Materials for Lithium-Ion Batteries Applications

Guanyu Wang, Tom Fearn, Tengyao Wang,* and Kwang-Leong Choy*

The electrochemical potentials of spinel lithium manganese oxide (LMO) have long been plagued by the significant Mn^{3+} dissolution during long cycle discharging, resulting in rapid capacity fading and short cycle life. Although the doping mechanisms are effective in suppressing these reactions, the correlations of their effects on the material properties and the improved discharging performance still remain uncovered. In this study, seven machine learning (ML) methods are applied to a manually curated dataset of 102 doped LMO spinel systems to predict the initial discharge capacities (IC) and 20th cycle end discharge capacities (EC) from fundamental system properties like material molar mass and crystal structure dimension. Gradient boosting models achieved the best prediction powers for IC and EC with their errors estimated to be 11.90 and 11.77 $mAhg^{-1}$, respectively. Besides, a higher formula molar mass of doped LMO can improve both capacities and additionally, a shorter crystal lattice dimension with a dopant with smaller electronegativity can slightly improve the value of the IC and EC, respectively. This study demonstrates the great potential of using ML models to both predict the discharging performance of doped spinel cathodes and identify the governing material properties for controlling the discharging performance.

1. Introduction

Rechargeable lithium-ion batteries (LIBs) are known as the most promising energy storage technology due to their high energy density, high power density, and long charge/discharge life cycle.[1,2] Presently, an extensive amount of research has been devoted to boosting their performance as to complement the applications in sustainable energy power and this demands for the improvements in storage capacity, steadiness and safety, toxicity, eco-friendliness, and material cost.[3–7] For this, discovering new cathode materials has become the key as they both contribute to 33% of the total battery cost and compared with the anode, have much lower storage capacity, and therefore greatly limit on the battery discharging capacities.

Among all cathode materials, spinel cathode materials ($LiMn_2O_4$) are preferred over the widely commercialized lithium cobalt oxide ($LiCoO_2$) material for its nontoxic nature, robust 3D structure (high Li-ion diffusion), and low cost (manganese metal is more abundant than cobalt metal). However, the issues of drastic capacity fading and limited rate performance have restricted their use in large-scale commercial applications. These inferior properties can be explained by two underlying chemical phenomena. The first is the dissolution of the manganese ions Mn^{3+} from the material surface into various forms of Mn^{4+}(solid) and Mn^{2+}(sol), which reduces the Li-ions site energy and eventually lowers the rate of reversible electrochemical reactions. The second reason is the Jahn–Teller distortion (JRD) effects initialized from the high spin electrons interactions from the d-orbital electrons of manganese ion (Mn^{3+}), which destabilize the overall crystal structure and hence reduce the respective cycle life.

Doping the manganese (III) sites with lower valence (lower than 3+) dopants (**Figure 1**a) seems to be an effective approach to this problem as it increases the average Mn valence in $LiMn_2O_4$ to suppress the JTD effect through reducing the concentration of Mn (III) and eventually decrease the rate of dissolution reaction. Indeed, promising results have been seen in capacity improvement for lower valence dopants such as Al,[8] Cr,[9] Fe,[10] Gd,[11] Ga,[12] Mg,[13] Nd,[14] Ni,[15] Ru,[16] Sc,[17] and Zn;[18] however, the use of higher valence dopants such as Si[19] and Sn[20] are also shown to be effective. Figure 1b shows

G. Wang
Institute for Materials Discovery
University College London
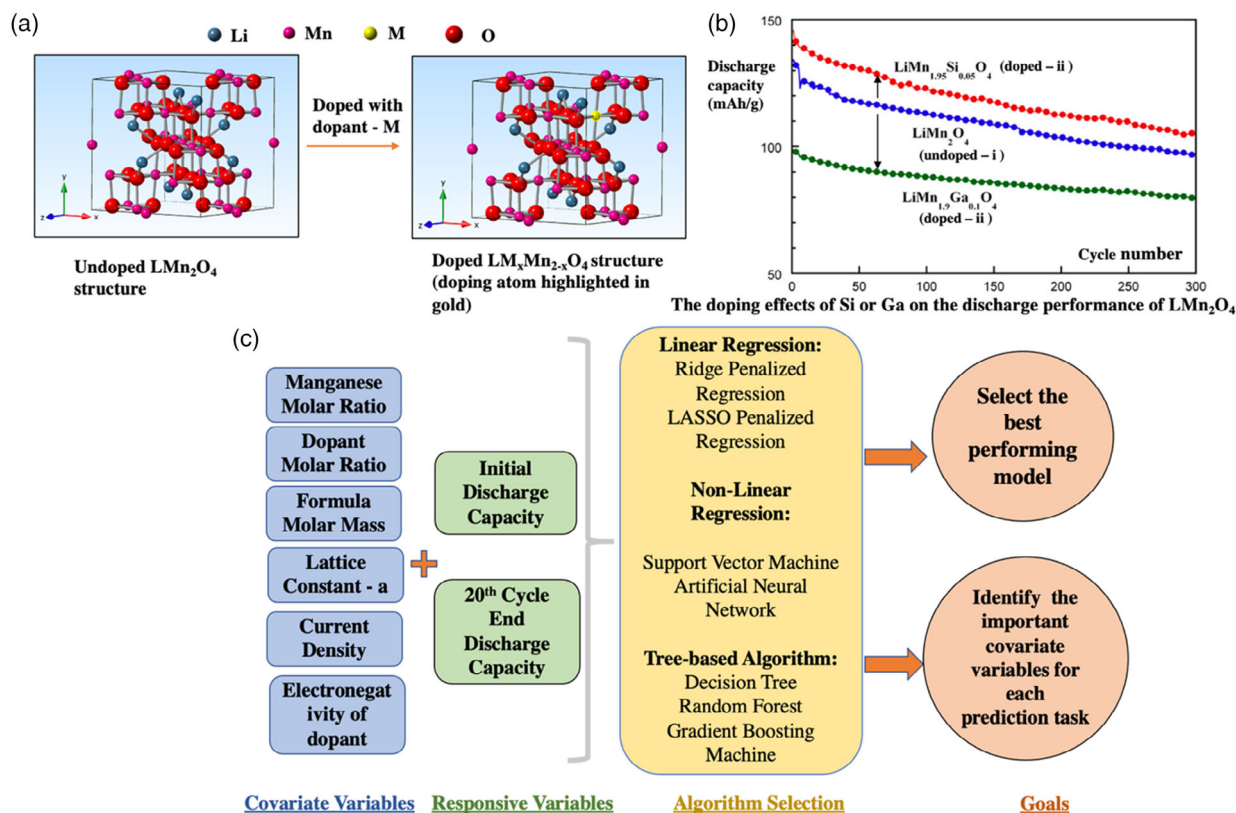Roberts Building, London WC1E 7JE, UK

Prof. T. Fearn, Dr. T. Wang
Department of Statistical Science
University College London
1-19 Torrington Place, London WC1R 7HB, UK
E-mail: tengyao.wang@ucl.ac.UK

Prof. K.-L. Choy
Institute for Materials Discovery
Faculty of Maths and Physical Sciences
University College London
Roberts Building, London WC1E 7JE, UK
E-mail: k.choy@ucl.ac.uk

The ORCID identification number(s) for the author(s) of this article can be found under https://doi.org/10.1002/ente.202100053.

ADVANCED
SCIENCE NEWS
www.advancedsciencenews.com

Energy Technology
Generation, Conversion, Storage, Distribution
www.entechnol.de

Figure 1. a) A schematic demonstration of the doping mechanism with the example dopant (M) for the pristine crystal structure of $LiMn_2O_4$ (LMO). b) The cyclic performances of the silicon-doped LMO, gallium-doped LMO, and the pristine LMO material; arrows indicate the performance gap. Reproduced with permission.[33] Copyright 2020, Elsevier. c) A summary of the model architecture, investigating algorithms and the final goals of selecting the best performing model as well as identifying the key features for predictions.

that the high-valence silicon-doped lithium manganese oxide (LMO) material offers a higher discharge capacity on the 60th cycle than both the lower valence gallium-doped system and the pristine material. This seems contradictory to the widely known doping principles because the introduction of high-valence dopants would increase the Mn valence in the system, leading to faster manganese (III) dissolution reactions and eventually worsen the cycling performance. From this, one can see that a comprehensive understanding in the doping mechanism and corresponding benefits on the spinel discharging capability are still lacking in the research community. One of the main root causes is the difficulty in comparing the results across different groups as there are a lot of variations in the experimental parameters such as synthesis routines, doping concentration, and testing conditions. The current study aims to uncover the underlying relationships of these complex material properties with the corresponding electrochemical properties using machine learning (ML) techniques.

ML algorithms have received a tremendous amount of interest in recent years due to their robust analytical and predictive abilities. One important benefit is it allows the researchers to gain valuable insights into intercorrelations between multiple variables that are too complex to be understood by pairwise examination of the variables. The implementations of ML in battery material research are seen to be growing at a significant rate.

Min et al.[21] built a random forest model that can capture 75% of the variation in the capacity retention rate of nickel–manganese–cobalt cathode materials from using the material synthesis parameters. Joshi et al.[22] concluded that deep learning model is powerful in predicting the voltage of electrode materials for different metal-ion batteries with nearly 81% of the variations being captured in a holdout test dataset. Furthermore, Zhang et al.[23] implemented clustering algorithms to group the Li-containing compounds' X-ray diffraction spectroscopy patterns according to their ionic conductivity and this eventually led to the discovery of 16 new conductors with the conductivities range of 10^{-4}–10^{-1} S cm^{-1}. Other successful cases are also seen in predicting the cathodes crystal system[24] and the remaining useful life of the LIB[25] and also to detect the LIB cell cracks.[26]

The discharge capacity at a certain cycle is not a quantity that can be derived by any existing physical models and the experimental measures are often very difficult to control due to the presence of many independent parameters. In this study, the aim is to investigate the potentials of using ML to predict the initial and 20th cycle end discharge capacity for doped spinel systems from various reported material properties, including the ICP molar ratio for dopant (M) and manganese atom (Mn) in the material, crystal lattice constant-a (LC_a), elemental properties such as the material molecular mass (M), dopant's electronegativity (M_EN), as well as the experimental condition—current

**ADVANCED
SCIENCE NEWS**
www.advancedsciencenews.com

Energy Technology
Generation, Conversion, Storage, Distribution

www.entechnol.de

density (CD). A summary of the model variable selection is shown in Figure 1c. First, seven multivariate models are built for each prediction task and this covers a wide range of linear and nonlinear algorithms such as the ridge regression (RR), lasso regression (LR), support vector machine (SVM), deep neural network (DNN), decision-tree (DS), random forest (RF), and the gradient boosting model (GBM). The principles and theories of these models can be widely found in other literature and will not be further discussed here.[27] Next, a variable importance study is performed, with the best performing tree-based models, to gain valuable insights into the governing material properties on the discharging performance.

2. Results and Discussion

The distributions of collected IC and EC values of 102 doped spinel cathodes are shown in Figure S1, Supporting Information. Their ranges are 50.8–149.0 and 43.33–134.89 mAh g^{-1}, respectively. **Figure 2** shows the matrix results of the Pearson coefficient correlation study performed for each pair of variables in the dataset. The level of statistical confidence of these calculated coefficient values is also shown in Figure S3, Supporting Information. The Pearson correlation coefficient (R) values are presented in the range of 0 and 1, with the value closer to either −1 (darker blue) or 1 (darker red), implying a more positive or negative linear relationship between the investigating variable pair. From the results presented, one's intuition should not be misguided by the perfect negative linearity ($R = -1$) relationship estimated for the M and Mn as it is the result of direct site substitution. In addition, Mr is found to have a relatively stronger linear correlation with IC and with EC than other pairs with coefficients estimated to be $R = 0.38$ and $R = 0.35$, respectively. To conclude, there are no strong linear correlations ($R > 0.6$)
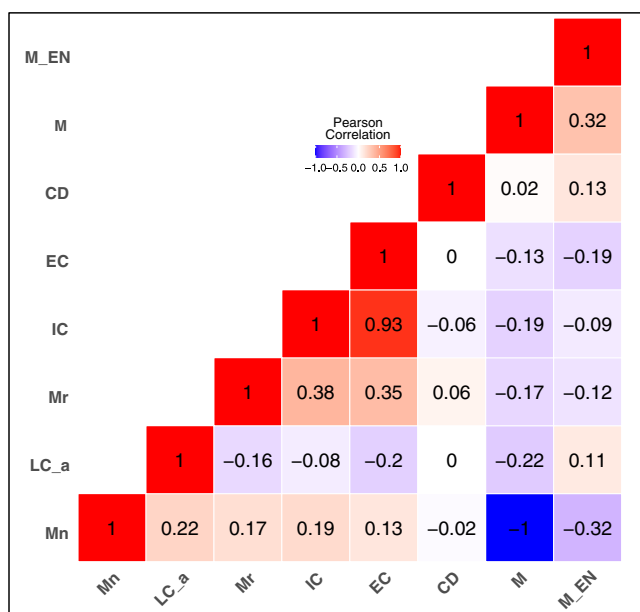
Figure 2. Result matrix of the Pearson correlation coefficient of every variable pair including the responsive variables, IC and EC, and the covariate variables, LC_a, Mn, M, M_electron, and CD.
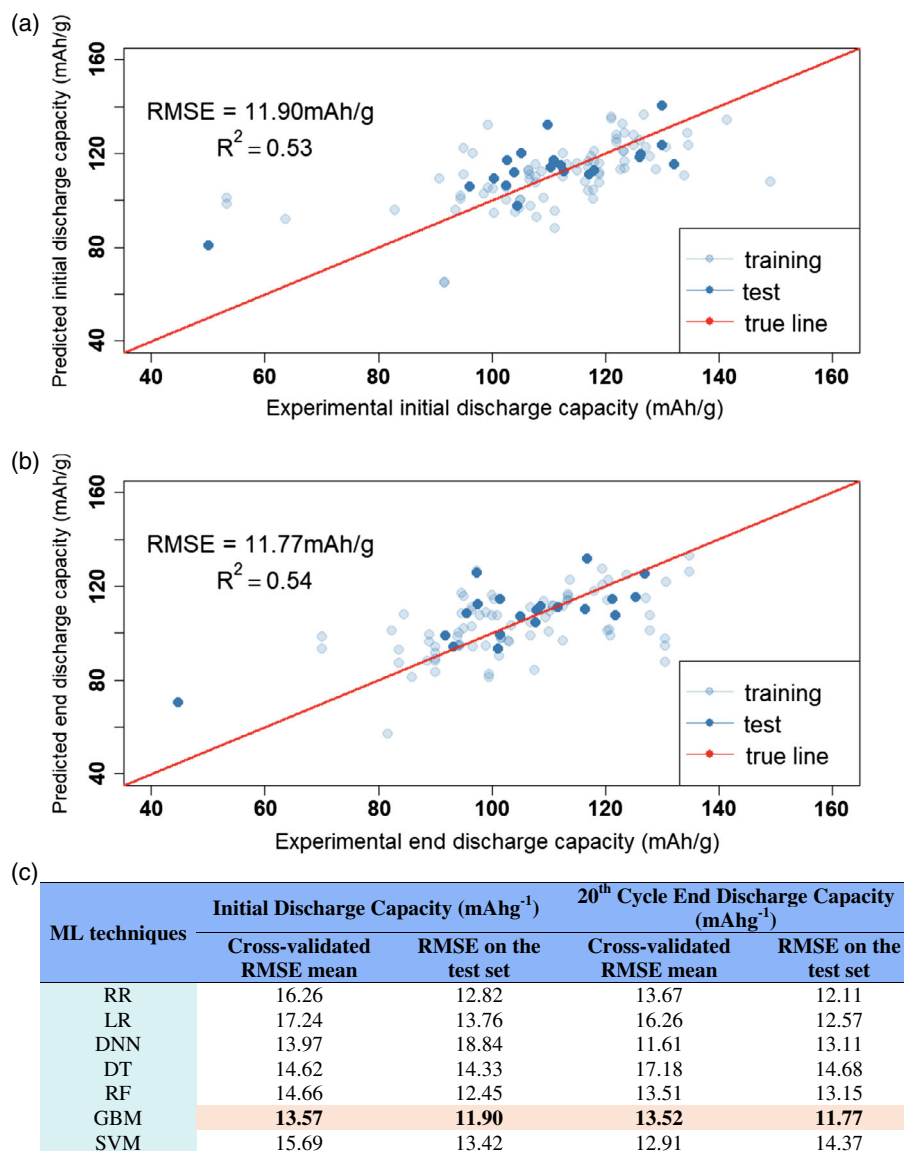
being observed for any of the covariate (M, Mn, LC_a, CD, M_EN) with the two response variables (IC, EC).

Finding a suitable ML algorithm is crucial for capturing the accurate underlying relationship between material properties and the discharging performance. Figure 2c shows the estimated mean root mean square error (RMSE) through tenfold cross-validated training and the predictions against the holdout dataset. Among all models, the GBM model has shown the best performance in generalizing for both the initial and 20th cycle end discharge capacities, with the RMSE calculated to be 11.90 and 11.77 mAh g^{-1} from the test set predictions. In addition, the cross-validated RMSE mean value for each prediction is observed to be higher than the test set RMSE values, which imply that the models are not encountering overfitting issues. It is important to note that the RMSE test set value shows more of the model's true prediction power because the test set data are not involved in the model training process. In this respect, GBM models will be chosen for further analysis as they have the lowest test set RMSE values in each case.

Gradient boosting algorithm is an ensemble approach where the base tree learners are built sequentially to minimize the residual errors from every previous training iteration. The advantages of the gradient boosting algorithm are seen from its robustness in predicting nonlinear relationships, offering more flexible hyperparameter tuning options (minimum tree depth, learning rate, number of iterations) and not requiring data preprocessing prior to the model training. With the aid of GBM approach, promising results are seen in screening out the feasible solid electrolyte for dendrite growth suppression,[28] predicting the bandgaps and heat of formation for Pb-free halide perovskites,[29] and predicting the efficiency of organic solar cells.[30]

For the given experimental dataset, GBM are seen to hold the best prediction power for both prediction tasks. Figure 2a,b shows the linearity plots for both the training set and test set of initial and end discharge capacity predictions as well as their respective RMSE, R^2 values on the test set. The plots have demonstrated the reasonable linearities for the predicted capacities and experimental capacities on both training and test set. In addition, both GBMs can produce good predictions against the test set without showing any noticeable sign of overfitting to the training data. However, a few outliners (data out of the normal distribution) can be identified at the lower range of the discharge capacity (smaller than 80 mAh g^{-1}) for both plots and this has affected the R^2 scores (**Figure 3**).

Most nonlinear algorithms such as neural network and support vector machine are known as the "black-boxes" as they do not provide any valuable insights into the approximated internal functions for the prediction task. On the contrary, the gradient boosting algorithm explains variable importance because of the highly interpretable nature of the DS. **Figure 4**a shows the relative importance of the six covariate variables for both prediction tasks and there are no redundant variables involved in the model considering all values are above zero. First, the molar mass of the doped LMO is observed to be the most important variable for the predictions of IC and EC prediction with their relative importance estimated as 37.44 and 36.05, respectively. For this, Faraday's law stated that the material molar mass and the number of reactive electrons/Li ions in the electrochemical reactions are reversely proportionally to the

**ADVANCED
SCIENCE NEWS**

www.advancedsciencenews.com

Energy Technology
Generation, Conversion, Storage, Distribution

www.entechnol.de

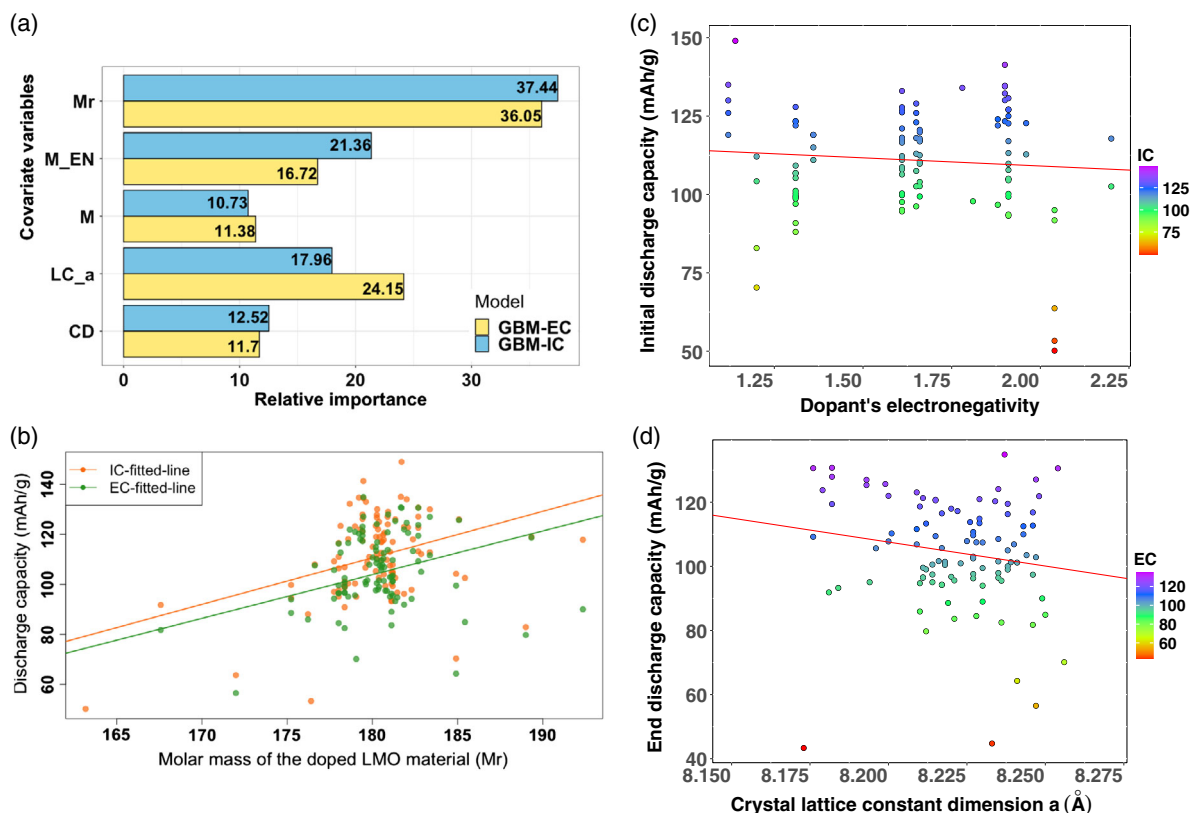| ML techniques	Initial Discharge Capacity (mAhg⁻¹)		20ᵗʰ Cycle End Discharge Capacity (mAhg⁻¹)	
	Cross-validated RMSE mean	RMSE on the test set	Cross-validated RMSE mean	RMSE on the test set
RR	16.26	12.82	13.67	12.11
LR	17.24	13.76	16.26	12.57
DNN	13.97	18.84	11.61	13.11
DT	14.62	14.33	17.18	14.68
RF	14.66	12.45	13.51	13.15
GBM	**13.57**	**11.90**	**13.52**	**11.77**
SVM	15.69	13.42	12.91	14.37

Figure 3. a) Scatter plots of experimental values against the predicted value for initial capacity and b) 20th cycle end capacity performed by the GBM. c) The mean RMSE values for during the tenfold cross-validation and for testing against 20 holdout test dataset for the prediction of Initial discharge capacity and end discharge capacity.

specific capacity of an electrode (the ideal amount of energy available for withdrawing per unit mass). In this regard, the variation in material molar mass would inevitability influence the practical capacities on both the first and the 20th discharging cycle as they are quantitively related to the specific capacity. Figure 4b shows positive linearity trends for the material molar mass with both discharging capacities in the whole dataset and this might suggest that the higher molar mass of doped LMO formula can lead to higher values for IC and EC.

The electronegativity and the lattice constant(*a*) of the dopant atom are determined to be the second most important variable for the IC and the EC predictions and their relative importance estimated to be 21.36 and 24.15, respectively. The electronegativity of the dopant can modify the overall structural density of the

doped LMO systems as it controls the bonding strength with the surrounding manganese ions and oxygen ions. A small difference in the electronegativity value indicates the formation of covalent bonds, which, in turn, makes the structure more stable and less dense than the structure that contains ionic bonds. In addition, the Li-ion site energy would be changed according to the modified structural density, and this would change the rate of intercalation/deintercalation of the Li ions from the LMO cathode, resulting various loading capacities at the first cycle. Figure 4c shows a negative correlation between IC and the dopant's electronegativity, with the highest capacities occurring at the lowest electronegativity value. However, this correlation is not conclusive due to the dispersed distribution. In addition, variations in the crystal lattice dimension of the doped LMO

ADVANCED
SCIENCE NEWS
www.advancedsciencenews.com

Energy Technology
Generation, Conversion, Storage, Distribution

www.entechnol.de

Figure 4. a) The relative importance of the model input variable for the prediction of the initial (IC) and the 20th cycle end discharge capacity (EC) estimated by the optimized GBMs. b) The plot of the values of IC and EC against the molar mass of the doped LMO cathode material with the linearity fitted lines for the whole dataset. c) The plot of IC against dopant's electronegativity with the red best-fitted line. d) EC versus crystal lattice constant-*a* with the red best-fitted line.

cathode would also influence the Li-ion site energy which is highly correlated to the discharging performance of the 20th cycle. For this, previous studies have confirmed the important influence of the crystal lattice parameters on the discharging performance of manganese such as the doped spinel(LiMg$_x$Mn$_{2-x}$O$_2$),[31] and the finding was made such as the larger crystal lattice dimension often leading to poor discharging performance in the short cyclic run and this was reconfirmed by the negative slope best-fitted line, as shown in Figure 4d.

Despite the promising results as seen from the model prediction performance, there are still many remaining challenges remained in curating perfectly comparable data for ML model construction. First, considerable variations are observed in the battery cell fabrication methods such as the mixing ratio for the anode and cathode components (e.g., binder, conductive additives, and active material). This variation is due to the lack of commonly agreed experimental standards across different research teams and thereby is varied case-by-case. The ratio of binder and additive can affect the mechanical stability and the conductivities of the cathode material; therefore, this would have an impact in predicting the long-term discharge capacities.[32] However, due to the complexity in curating such information while considering that the active LMO component being the main driving force for the electrochemical reactions, such mixing ratio is assumed to be standardized during the data collection

and is not involved in the model construction. Second, the microstructure of the cathode material such as particle sizes and their distribution as well as their surface morphologies are known to be affecting the conductivity and the rate of electrochemical reactions of the cathode.[8–34] The complication of such data is found to be challenging as either the measurements are not performed in some publication or the results are not published in the numerical format and would require further interpretation. Similar issues and challenges have also been encountered by Kauwe et al. during the data collection work for their data collection studies of LIB materials.[35] Lastly, despite a strict measure was made on collecting data from battery cells that used organic LiPF$_6$ electrolyte cells, there is still a variation in the solvents used for this compound, ranging from ethylene carbonate, ethylene methylene carbonate, to dimethyl carbonate.

The standardization of the battery assembling and testing methods used in cathode research work is crucial for curating highly comparable data and subsequently to be used for producing accurate predictive ML models. There are still many aforementioned independent variables in the dataset despite the great effort that has been made in filtering and selecting the publications with the highest comparability. In this perspective, we have additionally summarized the following improvement points for the experimental and data scientist researchers to consider as the future work to enhance the power of the ML

ADVANCED
SCIENCE NEWS
www.advancedsciencenews.com

Energy Technology
Generation, Conversion, Storage, Distribution

www.entechnol.de

approach: 1) Standardize the cell fabrication methods for anode, cathode, electrolyte, and report the experimental parameters in detail, including the mixing ratio of the raw materials. 2) Report the full results of the electrode features such as the X-ray diffraction (XRD) results, physical dimensions, crystal structure distribution, particle size and their distribution, and the pore sizes in "csv" format so that it would be more assessable to ML models. 3) Use the principal component analysis method to reduce the dimensions of the descriptor space prior to the model training to improve the training speed and prediction accuracy. 4) Discover new descriptors for describing the material properties, for example, using density functional theory to estimate the dipole moment.

3. Conclusions

To conclude, we have explored the scope of seven algorithms for their prediction power in describing the correlations of six different structural and elemental properties of 102 doped LMO systems and the corresponding discharging performance at the first and 20th cycles. The dataset was carefully curated from the literature, with data collection rules such as the standardized experimental conditions (i.e., electrolyte, anode, discharging environment temperature) being applied to ensure achieve good quality data. Out of the seven investigated algorithms, the GBM algorithm demonstrated the best predicting power for IC and EC with the RMSE for each being the lowest from the validation against the heldout test set. A variable importance study was conducted using the GBM models and the results suggest that a higher molar mass of doped LMOs can lead to a higher discharge capacity. In addition, weak negative correlations are captured for the variable pair of the electronegativity of the dopant in LMO with IC and for the crystal structure lattice constant-*a* with EC, respectively. The results of this study have demonstrated the great potentials in implementing ML algorithms to grasp the complex structure–property correlations of the doped LMO systems which could shorten the testing duration of battery material performance and leading a faster discovery speed of new doped cathode materials for LIBs with higher storage capacity and longer life cycle.

4. Experimental Section

Data Collection of the Doped Spinel Materials: The dataset consisted of 102 different doped spinel systems with 17 dopant variations (B, Co, Ni, Al, Cr, Ce, Sc, Mg, Gd, Zn, Si, Sn, Nd, Ga, Co, In, and Ru) and was curated from over 34 reliable publications between 1998 and 2019. A broad range of covariate variables were selected from the material properties (M, Mn, LC_a, Mr, M_and EN) and the experimental condition (CD). The materials' discharging properties such as IC and EC were extracted from cyclic result graph using graphic extraction algorithms. For material properties, data collections were strictly made for single doped, noncoated spinel cathode system with a space group of *Fd-3 m* and any materials that were indicated as oxygen-deficient or used anion doping like fluoride were discarded. The purpose of this was to maintain a high consistency of the material data for better model training. For collecting the results of discharge capacities, the cyclic performance test must fulfill all listed conditions: 1) used lithium foil as the contrasting anode; 2) used aqueous $LiPF_6$ as the electrolyte; 3) used the charge/discharge CD to be within $150\,mAh\,g^{-1}$, also called 1 C (the discharge current will discharge the full

charged battery within 1 h); 4) a minimum of performance of 20 charges/ discharge cycles; and 5) performed the cyclic test under standard room conditions ($T = 25\,°C$, $P = 1\,atm$). The 20th cycle discharge capacity was selected as the collection target as it was the most commonly performed cycle across the literature. A schematic illustration of the data collection rules used for each step of the collection process is shown in Figure S2, Supporting Information.

Model Training: The ML models used in this work were implemented using various R (version 3.6.0) libraries, including caret, gbm, randomForest, and keras. The whole data space was randomly split into the ratio of 4:1, which corresponds to the model training set and test set. Model hyperparameters were optimized using tenfold cross-validation during model training and the results are shown in Table S1, Supporting Information.

Model Evaluation Metrics: The evaluation of model performance will be mainly assessed through the calculation of the RMSE and of the coefficient of determination (R^2) from the predictions against the formerly split holdout test set. The calculations of each are given as Equation (1) and (2) as follows

$$RMSE = \sqrt{\frac{1}{n}\sum_{i=1}^{n}(y_i - \hat{y}_i)^2} \tag{1}$$

$$R^2 = 1 - \frac{\sum_{i=1}^{n}(y_i - \hat{y}_i)^2}{\sum_{i=1}^{n}(y_i - \bar{y})^2} \tag{2}$$

where n is the number of values, y_i is the observed variable, $\hat{y}_i$ is the predicted values, and $\bar{y}$ is the average of the observed values.

Supporting Information

Supporting Information is available from the Wiley Online Library or from the author.

Acknowledgements

All authors contributed equally to this work.

Conflict of Interest

The authors declare no conflict of interest.

Data Availability Statement

The collected data used for constructing these machine learning algorithms are available on the GitHub page (https://github.com/thepowerligand/LMO_ML/blob/main/LMO.csv). The references for these selected journals are given as S3 in supporting information.

Keywords

[1] S. Amjad, S. Neelakrishnan, R. Rudramoorthy, *Renew. Sustain. Energy Rev.* **2010**, *14*, 1104.
[2] G. Ren, G. Ma, N. Cong, *Renew. Sustain. Energy Rev.* **2015**, *41*, 225.

[3] L. Lu, X. Han, J. Li, J. Hua, M. Ouyang, *J. Power Sources* **2013**, *226*, 272.

[4] J. Wen, Y. Yu, C. Chen, *Mater. Express* **2012**, *2*, 197.

[5] T. M. Bandhauer, S. Garimella, T. F. Fuller, *J. Electrochem. Soc.* **2011**, *158*, R1.

[6] P. Arora, *J. Electrochem. Soc.* **1998**, *145*, 3647.

[7] A. Evans, V. Strezov, T. J. Evans, *Renew. Sustain. Energy Rev.* **2012**, *16*, 4141.

[8] W. H. Ryu, J. Y. Eom, R. Z. Yin, D. W. Han, W. K. Kim, H. S. Kwon, *J. Mater. Chem.* **2011**, *21*, 15337.

[9] Z. D. Peng, Q. L. Jiang, K. Du, W. G. Wang, G. R. Hu, Y. X. Liu, *J. Alloys Compd.* **2010**, *493*, 640.

[10] H. Liu, R. Tian, Y. Jiang, X. Tan, J. Chen, L. Zhang, Y. Guo, H. Wang, L. Sun, W. Chu, *Electrochim. Acta* **2015**, *180*, 138.

[11] P. Ram, A. Gören, S. Ferdov, M. M. Silva, G. Choudhary, R. Singhal, C. M. Costa, R. K. Sharma, S. Lanceros-Méndez, *Solid State Ionics* **2017**, *300*, 18.

[12] S. C. Han, S. P. Singh, Y. Hwang, E. G. Bae, B. K. Park, K.-S. Sohn, M. Pyo, *J. Electrochem. Soc.* **2012**, *159*, A1867.

[13] J. Huang, F. Yang, Y. Guo, C. Peng, H. Bai, J. Peng, J. Guo, *Ceram. Int.* **2015**, *41*, 9662.

[14] R. Singhal, S. R. Das, M. S. Tomar, O. Ovideo, S. Nieto, R. E. Melgarejo, R. S. Katiyar, *J. Power Sources* **2007**, *164*, 857.

[15] Y. Duan, J. Guo, M. Xiang, J. Zhu, C. Su, X. Bai, X. Liu, W. Bai, R. Wang, *Solid State Ionics* **2018**, *326*, 100.

[16] M. V. Reddy, S. S. Manoharan, J. John, B. Singh, G. V. Subba Rao, B. V. R. Chowdari, *J. Electrochem. Soc.* **2009**, *156*, A652.

[17] Y. Xie, Y. Xu, L. Yan, Z. Yang, R. Yang, *Solid State Ionics* **2005**, *176*, 2563.

[18] P. Chand, V. Bansal, S. V. Singh, *Mater. Sci. Eng. B Solid-State Mater. Adv. Technol.* **2018**, *93*, 238.

[19] H. Zhao, X. Liu, C. Cheng, Q. Li, Z. Zhang, Y. Wu, B. Chen, W. Xiong, *J. Power Sources* **2015**, *282*, 118.

[20] S. Guo, S. Zhang, X. He, W. Pu, C. Jiang, C. Wan, *J. Electrochem. Soc.* **2008**, *155*, A760.

[21] K. Min, B. Choi, K. Park, E. Cho, *Sci. Rep.* **2018**, *8*, 1.

[22] R. P. Joshi, J. Eickholt, L. Li, M. Fornari, V. Barone, J. E. Peralta, *ACS Appl. Mater. Interfaces* **2019**, *11*, 18494.

[23] Y. Zhang, X. He, Z. Chen, Q. Bai, A. M. Nolan, C. A. Roberts, D. Banarjee, T. Matsunaga, Y. Mo, C. Ling, *Nat. Commun.* **2019**, *10*, 1.

[24] M. Attarian Shandiz, R. Gauvin, *Comput. Mater. Sci.* **2016**, *117*, 270.

[25] Y. Zhang, R. Xiong, H. He, M. G. Pecht, *IEEE Trans. Veh. Technol.* **2018**, *67*, 5695.

[26] L. Petrich, D. Westhoff, J. Feinauer, D. P. Finegan, S. R. Daemi, P. R. Shearing, V. Schmidt, *Comput. Mater. Sci.* **2017**, *136*, 297.

[27] M. Kuhn, *J. Stat. Softw.* **2008**, *28*, 1.

[28] Z. Ahmad, T. Xie, C. Maheshwari, J. C. Grossman, V. Viswanathan, *ACS Cent. Sci.* **2018**, *4*, 996.

[29] J. Im, S. Lee, T. W. Ko, H. W. Kim, Y. K. Hyon, H. Chang, *Npj Comput. Mater.* **2019**, *5*, 1.

[30] H. Sahu, W. Rao, A. Troisi, H. Ma, *Adv. Energy Mater.* **2018**, *8*, 1801032.

[31] M. Xiang, C. W. Su, L. Feng, M. Yuan, J. Guo, *Electrochim. Acta* **2014**, *125*, 524.

[32] S. Hein, T. Danner, D. Westhoff, B. Prifling, R. Scurtu, L. Kremer, A. Hoffmann, A. Hilger, M. Osenberg, I. Manke, M. Wohlfahrt-Mehrens, V. Schmidt, A. Latz, *J. Electrochem. Soc.* **2020**, *167*, 013546.

[33] A. Iturrondobeitia, A. Goñi, V. Palomares, I. Gil De Muro, L. Lezama, T. Rojo, *J. Power Sources* **2012**, *216*, 482.

[34] J. Mao, K. Dai, M. Xuan, G. Shao, R. Qiao, W. Yang, V. S. Battaglia, G. Liu, *ACS Appl. Mater. Interfaces* **2016**, *8*, 9116.

[35] S. Kauwe, T. Rhone, T. Sparks, *Crystals* **2019**, *9*, 54.